Journal of Pharmaceutical Analysis 14 (2024) 211–224

Contents lists available at ScienceDirect

Journal of Pharmaceutical Analysis

journal homepage: www.elsevier.com/locate/jpa

Original article

Pyrimethamine upregulates BNIP3 to interfere SNARE-mediated autophagosome-lysosomal fusion in hepatocellular carcinoma

Jingjing Wang, Qi Su, Kun Chen, Qing Wu, Jiayan Ren, Wenjuan Tang, Yu Hu, Zeren Zhu, Cheng Cheng, Kaihui Tu, Huaizhen He, Yanmin Zhang*

School of Pharmacy, Health Science Center, Xi'an Jiaotong University, Xi'an, 710061, China

ARTICLE INFO

Article history:
Received 7 April 2023
Received in revised form
13 May 2023
Accepted 29 May 2023
Available online 1 June 2023

Keywords:
Pyrimethamine
BNIP3
SNARE
Autophagosome-lysosome fusion
Hepatocellular carcinoma
Sorafenib

ABSTRACT

Hepatocellular carcinoma (HCC) is one of the most common tumor types and remains a major clinical challenge. Increasing evidence has revealed that mitophagy inhibitors can enhance the effect of chemotherapy on HCC. However, few mitophagy inhibitors have been approved for clinical use in humans. Pyrimethamine (Pyr) is used to treat infections caused by protozoan parasites. Recent studies have reported that Pyr may be beneficial in the treatment of various tumors. However, its mechanism of action is still not clearly defined. Here, we found that blocking mitophagy sensitized cells to Pyr-induced apoptosis. Mechanistically, Pyr potently induced the accumulation of autophagosomes by inhibiting autophagosome-lysosome fusion in human HCC cells. *In vitro* and *in vivo* studies revealed that Pyr blocked autophagosome-lysosome fusion by upregulating BNIP3 to inhibit synaptosomal-associated protein 29 (SNAP29)-vesicle-associated membrane protein 8 (VAMP8) interaction. Moreover, Pyr acted synergistically with sorafenib (Sora) to induce apoptosis and inhibit HCC proliferation *in vitro* and *in vivo*. Pyr enhances the sensitivity of HCC cells to Sora, a common chemotherapeutic, by inhibiting mitophagy. Thus, these results provide new insights into the mechanism of action of Pyr and imply that Pyr could potentially be further developed as a novel mitophagy inhibitor. Notably, Pyr and Sora combination therapy could be a promising treatment for malignant HCC.

1. Introduction

Liver cancer is one of the most frequent fatal malignancies, and its fatality is ranked third among all diseases. Among all primary liver cancers, hepatocellular carcinoma (HCC) is the most common neoplasm [1], and immunotherapy and chemotherapy are currently the best curative options [2]. However, the occurrence of chemotherapy resistance [3] and immune escape [4] hinder attempts to control tumor growth. Therefore, new treatment options are necessary for patients with HCC.

In recent years, numerous studies have shown that autophagy plays a pivotal role in cancer treatment [5,6]. Autophagy is an important cellular homeostasis and cycling mechanism [7–10]. Initially, parts of the cytoplasm and organelles are engulfed within a double-membrane-bound vesicle called an autophagosome. The autophagosome fuses with lysosomes to form an autolysosome, which results in the degradation of sequestered materials by various lysosomal hydrolytic enzymes [11]. Substantial evidence suggests that soluble N-ethylmaleimide sensitive factor attachment protein receptor (SNARE) complexes are involved in autophagosome-lysosome fusion [12,13]. It has recently been reported that autophagosomal SNARE syntaxin 17 (STX17) interacts with cytosolic SNARE synaptosomal-associated protein 29 (SNAP29) and lysosomal SNARE vesicle-associated membrane protein 8 (VAMP8), all of which are required for autophagosome-lysosome fusion [14]. However, the molecular mechanism underlying the regulation of autophagosome-lysosome fusion is not fully understood.

The process of mitochondrial degradation through autophagy is called mitophagy, and it is important for mitochondrial quality control and homeostasis [15,16]. The mitophagy receptor BNIP3 is a protein homologous to Bcl-2 in its BH3 structural domain [17,18] and it may play an essential role in the fusion of autophagosomes with lysosomes [19,20]. However, the mechanistic function of BNIP3 in the regulation of autophagosome-lysosome fusion remains unclear. In addition, many studies have shown that mitophagy is necessary for the evolution of benign liver tumors to malignant HCC and that mitophagy promotes the occurrence and metastasis of HCC [21–23]. Given the important role of mitophagy

Peer review under responsibility of Xi'an Jiaotong University.
* Corresponding author.
E-mail address: zhang2008@mail.xjtu.edu.cn (Y. Zhang).

https://doi.org/10.1016/j.jpha.2023.05.014

in HCC progression, the search for inhibitors of mitophagy is essential to enhance the treatment of HCC.

Pyrimethamine (2,4-diamino-5-*p*-chlorophenyl-6-ethyl-pyrimidine; Pyr) is used for the treatment of infections caused by protozoan parasites [24,25]. In addition to antimalarial effects, recent studies have also reported that Pyr can treat different types of tumors, including lung cancer [26], melanoma [27,28], breast cancer [29], acute myeloid leukemia [30], and prostate cancer [31]. It has been suggested that the mechanism underlying the anti-cancer activity of Pyr involves the induction of cathepsin B-dependent and caspase-dependent apoptotic pathways, inhibition of STAT3, activation of caspase8/9, and cell cycle arrest in the S-phase. However, there are no reports of Pyr regulating mitophagy in human HCC cells.

In this study, we aimed to investigate the effects of Pyr on mitophagy and its underlying mechanism. We found that Pyr can effectively induce autophagosome accumulation by inhibiting the fusion of autophagosomes with lysosomes. *In vitro* and *in vivo* mechanistic studies revealed that Pyr blocks autophagosome-lysosome fusion by upregulating BNIP3 to inhibit SNAP29-VAMP8 interaction. In addition, we found that the combination of Pyr and sorafenib (Sora) had a synergistic effect, which was confirmed *in vitro* and *in vivo* through the observation that Pyr increased the sensitivity of human HCC cells to Sora by inhibiting mitophagy. These findings provide a new link between Pyr and mitophagy, which has clinical implications for potential HCC treatment strategies.

2. Materials and methods

All *in vivo* studies were performed using BALB/c male nude mice (4 weeks old, 18–22 g). All animal studies were conducted in accordance with the principles of the Institutional Animal Care and Use Committee. Moreover, the animal studies were performed under the permission of the Biomedical Ethics Committee (Approval number: 2021-1317) of the Department of Xi'an Jiaotong University Health Science Center. Please see the detailed materials and methods in the supplementary materials.

3. Results

3.1. Pyr inhibits the proliferation of HCC cells and induces apoptosis

At first, 3-(4,5-dimethylthiazol-2-yl)-2,5-diphenyltetrazolium bromide (MTT) assays were performed to investigate the effect of Pyr on the proliferation of HCC cell lines. Pyr inhibited the growth of HCC cells in a time- and concentration-dependent manner (Fig. 1A). Subsequent experiments were performed using HepG2 and SMMC-7721 cells, and the cytotoxicity of Pyr on SMMC-7721 and HepG2 cells was detected by Calcein-AM/PI double staining experiments. Notably, Fig. 1B shows that Pyr treatment led to HCC cell death. To further investigate whether Pyr enters HCC cells to exert anti-proliferative effects, the HPLC method was used to determine. Chromatograms obtained from the blank culture extraction solution and the blank extraction lysate (as a representative sample) are shown in Fig. S1. The standard curves for the relationship between the peak area of Pyr in quality-control samples and Pyr concentration were evaluated by least-squares regression analysis (Table S1). Within-run precision, between-run precision and extraction efficiency were determined for culture solution (Table S2) and lysate (Table S3) samples. These methods were then applied to determine the content of Pyr in supernatant liquid and cell lysate (Table S4). The results showed that the concentration of Pyr decreased in the cell supernatant liquid and increased in the cell lysate compared with the original concentration. In short, these results indicate that Pyr can inhibit the proliferation of SMMC-7721 cells by entering the cell.

Additionally, Pyr arrested HCC cells at S phase (Fig. S2), and the induction of apoptosis was observed by Annexin V/propidium iodide (PI) staining in Pyr-treated HCC cells (Figs. 1C and S3). Pyr reduced the expression of anti-apoptotic molecules, including Bcl-2, Mcl-1, and Bcl-X_L, and increased the expression of pro-apoptotic proteins (Bax and Bak), which suggests that Pyr induces apoptosis via mitochondrial pathways (Fig. 1D). Furthermore, caspases are central components of the machinery responsible for apoptosis [32–34]. Therefore, the levels of caspase family proteins were detected in HCC cells after Pyr treatment. As shown in Fig. 1E, caspase-8, caspase-9 and caspase-3 cleavage increased after Pyr treatment. Furthermore, cytochrome c (Cyto c) expression was increased and X-linked inhibitor of apoptosis (XIAP) expression was downregulated after Pyr treatment. The expression levels of apoptotic protease activating factor 1 (APAF-1), apoptosis-inducing factor (AIF), and poly(ADP-ribose) polymerase (PARP) cleavage increased after Pyr treatment (Fig. 1F). The levels of apoptosis-related proteins were also assessed at different time points, and the results indicated that the induction of apoptosis by Pyr was time-dependent (Fig. S4). Taken together, these results indicate that Pyr induces cell death via an intrinsic pathway mediated by Bcl-2 family proteins, APAF-1 oligomerization, AIF, and caspase activation.

3.2. Blocking autophagy sensitizes HCC cells to apoptosis induced by Pyr

Pyr treatment triggered cytoplasmic vacuolization in HCC cells (Fig. 1G). It has been reported that the vacuolization of cells is related to autophagy [35]; therefore, it is essential to investigate whether Pyr can influence autophagy. The expression of P62, Beclin 1 and light chain 3 (LC3)-II/LC3-I in HCC cells was detected by western blotting. Treatment of cells with Pyr resulted in the upregulation of these proteins (Figs. 1H and I). The increase in Beclin 1 expression after Pyr treatment indicated that Pyr could induce autophagy. Increased LC3-II/LC3-I ratios upon Pyr treatment confirmed an increase in autophagosomes. However, elevated P62 levels highlighted the blockage of late autophagy. Pyr induced greater accumulation of LC3-II when cells were co-activated with autophagy activator rapamycin (Rapa) (Figs. 1J and S5). Furthermore, the LC3-II/LC3-I ratio was assayed in the presence of the selective vacuolar (V)-ATPase inhibitor, bafilomycin (BafA1), the lysosomal inhibitor, chloroquine (CQ), and the mitophagy inhibitor, Mdivi-1. The combination of Mdivi-1 and Pyr significantly increased LC3-II conversion compared with single inhibitor treatment alone in both cell types (Figs. 1K and S6). These results suggest that Pyr blocks mitophagy, and taken together, these data indicate that Pyr is an autophagy activator that can block autophagic flux in the late stage. Treatment with BafA1, CQ, or Mdivi-1 increased Pyr-induced cell death (Fig. 1L) and apoptosis (Fig. 1M), indicating that autophagy, as a protective function, was reversed. In conclusion, these data demonstrate that Pyr induces apoptosis via autophagy.

3.3. Pyr initiates and blocks mitophagy

Mitochondrial morphology and function were assessed to evaluate mitochondrial alterations in Pyr-treated HCC cells. Mitochondria in Pyr-treated HCC cells were punctate compared to normal filamentous mitochondria in the control group (Fig. 2A). $\Delta\Psi m$ was significantly decreased in Pyr-treated cells compared to untreated cells, as shown in the tetramethylrhodamine ethyl ester (TMRE) assay (Fig. 2B). In addition, ATP levels and reactive oxygen species (ROS) production were measured after Pyr treatment to assess functional alterations. The ATP content in HCC cells decreased after Pyr treatment (Fig. 2C), while the ROS levels increased (Fig. 2D).

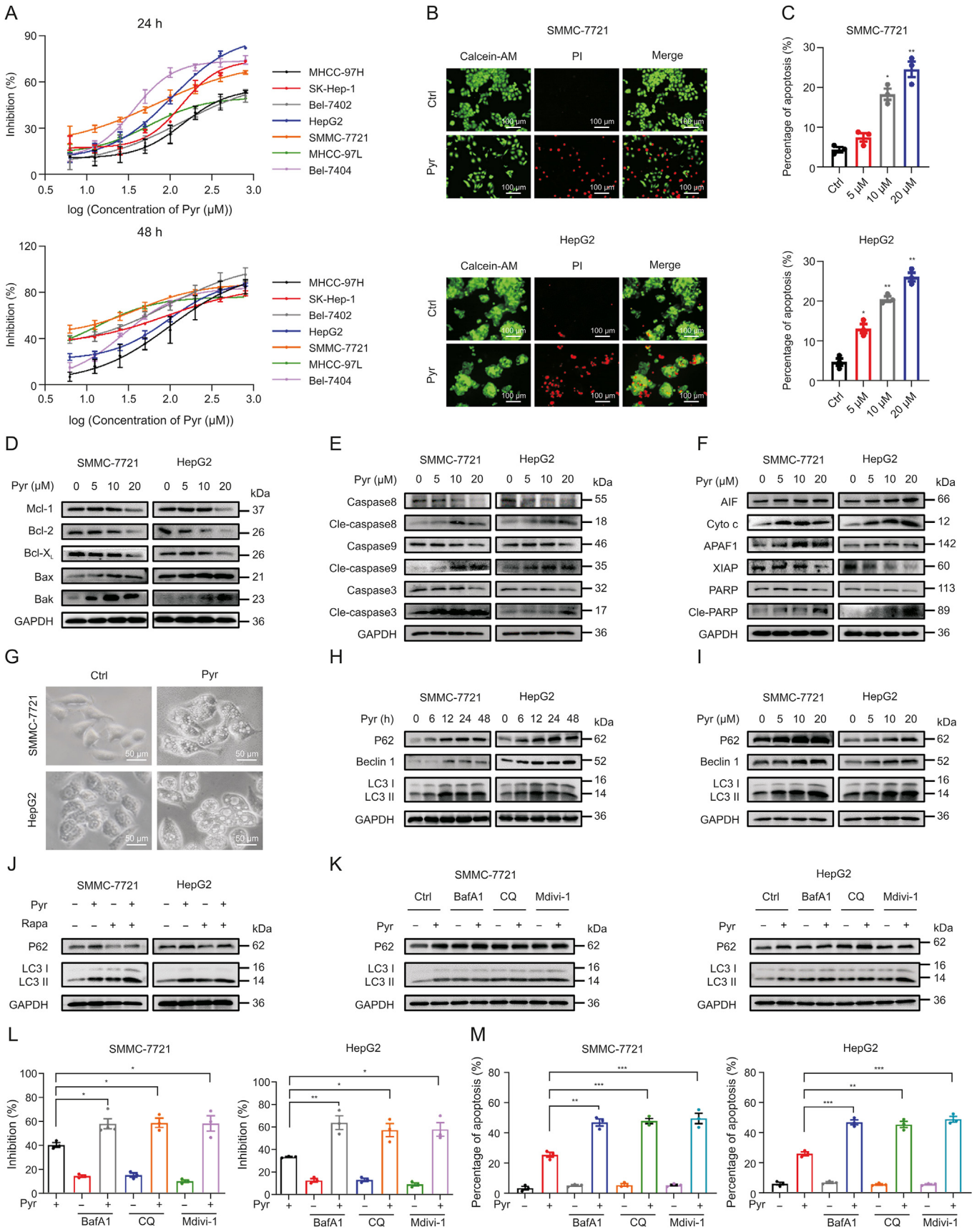

Fig. 1. Blocking autophagy sensitizes hepatocellular carcinoma (HCC) cells to pyrimethamine (Pyr)-induced apoptosis. (A) The effects of Pyr on HCC cell proliferation, were evaluated by 3-(4,5-dimethylthiazol-2-yl)-2,5-diphenyltetrazolium bromide (MTT) test ($n = 3$). (B) HCC cells were treated with 20 μM Pyr for 48 h. Representative images of Pyr cytotoxicity against HCC cells as assessed by Calcei-AM/propidium iodide (PI) double staining. ($n = 3$). (C) HCC cells were treated with Pyr for 48 h. Cell apoptosis was measured by

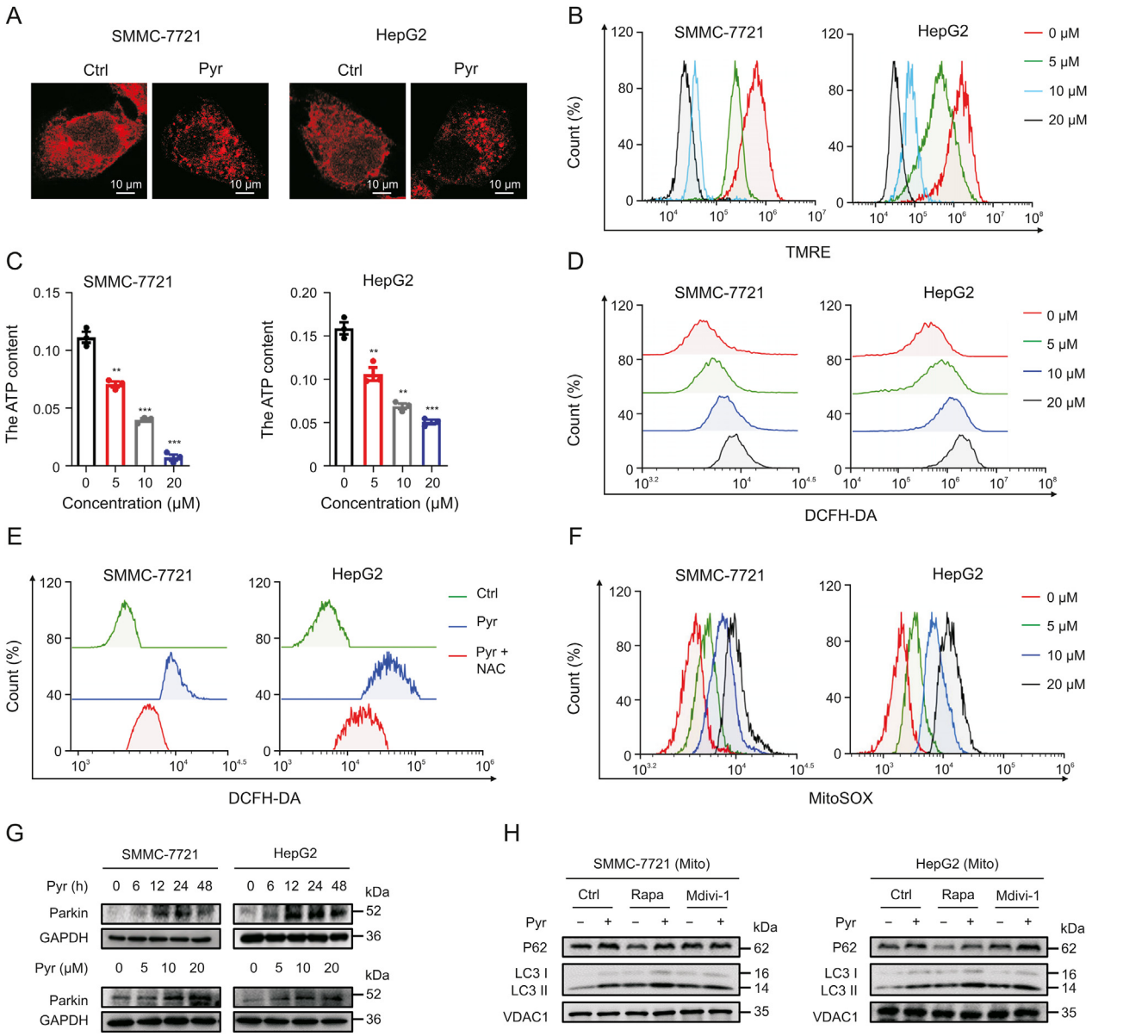

Fig. 2. Pyrimethamine (Pyr) initiates and blocks mitophagy. (A) Hepatocellular carcinoma (HCC) cells were treated with 20 μM Pyr for 12 h and stained with MitoOrange. (B) Changes in ΔΨm following treatment of HCC cells with Pyr were analyzed by tetramethylrhodamine ethyl ester (TMRE) staining and flow cytometry. ($n = 3$). (C) ATP content in HCC cells was assessed using an ATP Assay Kit. Data are presented as the mean ± standard deviation of the mean (SEM), $n = 3$. $^{**}P < 0.01$, $^{***}P < 0.001$. (D) HCC cells were labeled with a 2'-7'-Dichlorodihydrofluorescein diacetate (DCFH-DA) probe, and intracellularreactive oxygen species (ROS) levels were assessed using flow cytometry ($n = 3$). (E) HCC cells were treated with 20 μM Pyr alone or in combination with 5 mM NAC for 12 h. Cells were then labeled with a DCFH-DA probe, and intracellular ROS levels were quantified using flow cytometry ($n = 3$). (F) HCC cells were treated with Pyr for 12 h. The cells were then labeled with a MitoSOX probe, and the mitophagy-mediated ROS levels were measured using flow cytometry ($n = 3$). (G) Protein expression of Parkin in Pyr-treated HCC cells ($n = 3$). (H) HCC cells were treated with 20 μM Pyr in the presence of 20 nM bafilomycin (BafA1), 20 μM chloroquine (CQ), or 10 μM Mdivi-1 for 12 h. Then the mitochondrial fractions (Mito) were prepared, and autophagy-related protein expression in mitochondria were evaluated by western blotting. Voltage-dependent anion channel 1 (VDAC1) served as the control ($n = 3$). GAPDH: glyceraldehyde 3-phosphate dehydrogenase; LC3: light chain 3; Ctrl: control group.

Annexin V/PI staining, and the quantitation of apoptotic cells was shown. Data are presented as the mean ± standard deviation of the mean (SEM), $n = 3$. $^{*}P < 0.05$, $^{**}P < 0.01$. (D–F) HCC cells were treated with Pyr for 48 h. Apoptosis-related protein expression was examined by western blotting ($n = 3$). (G) Morphological effect of Pyr on HCC cells after treatment with 20 μM Pyr for 48 h. Extensive cytoplasmic vacuolization was induced with Pyr. ($n = 3$). (H) HCC cells were treated with 20 μM Pyr and autophagy-related protein expression was examined by western blotting ($n = 3$). (I) HCC cells were treated with Pyr for 12 h and autophagy-related protein expression was examined by western blotting ($n = 3$). (J) HCC cells were treated with 20 μM Pyr in the presence of 100 nM rapamycin (Rapa) for 12 h. Autophagy-related protein expression was examined by western blotting ($n = 3$). (K) HCC cells were treated with 20 μM Pyr in the presence of 20 nM bafilomycin (BafA1), 20 μM chloroquine (CQ), or 10 μM Mdivi-1 for 12 h. Autophagy-related protein expression was examined by western blotting ($n = 3$). (L) HCC cells were treated with 20 μM Pyr in the presence of 20 nM BafA1, 20 μM CQ, or 10 μM Mdivi-1. Cell cytotoxicity was analyzed using an MTT assay. Data are presented as the means ± SEM, $n = 3$. $^{*}P < 0.05$, $^{**}P < 0.01$. (M) Cell apoptosis was measured by Annexin V/PI staining in HCC cells treated with 20 μM Pyr in the presence of 20 nM BafA1, 20 μM CQ, or 10 μM Mdivi-1. Quantitation of apoptotic cells is shown. Data are presented as the mean ± SEM, $n = 3$. $^{**}P < 0.01$, $^{***}P < 0.001$. GAPDH: glyceraldehyde 3-phosphate dehydrogenase; AIF: apoptosis-inducing factor; Cyto c: cytochrome c; APAF1: apoptotic protease-activating factor 1; XIAP: X-linked inhibitor of apoptosis; PARP: poly(ADP-ribose) polymerase; LC3: light chain 3; Ctrl: control group.

Afterwards, the cells were pretreated with 5 mM NAC (a ROS scavenger), which reduced Pyr-induced intracellular ROS accumulation in HCC cells (Fig. 2E). Additionally, MitoSOX was used to measure mitochondrial ROS levels. As shown in Fig. 2F, the mitochondrial ROS levels in HCC cells increased after Pyr treatment. These results suggest that Pyr causes mitochondrial dysfunction.

Next, it was investigated whether HCC cells initiated mitophagy to remove dysfunctional mitochondria. Notably, the expression of Parkin, a key factor in mitophagy [36], markedly increased (Fig. 2G), which suggests that Pyr treatment promotes mitophagy. However, in mitochondrial proteins, Pyr induced a greater accumulation of LC3-II when cells were co-treated with Rapa. Additionally, combination treatment with Mdivi-1 and Pyr considerably increased LC3-II conversion in both HCC cell lines compared to the single inhibitor treatment (Fig. 2H). These data reveal that Pyr inhibits late mitophagy. Taken together, the results suggest that Pyr initiates and blocks mitophagy.

3.4. Pyr regulates mitophagy by interfering with autophagosome-lysosome formation

The above results indicate that Pyr inhibits autophagic flux during the late stages of autophagy. Thence, the effect of Pyr on lysosomal function was next investigated. Cathepsin B and D are the main lysosomal proteases, and their deficiency leads to impaired autophagy [37,38]. It is worth noting that Pyr increased the levels of the mature forms of cathepsin B and cathepsin D (Fig. 3A), which indicates that Pyr does not affect autophagy by affecting the maturation of lysosomal enzymes. Lysosomal associated membrane protein 1 (LAMP1) is a crucial component of the lysosomal membrane and its protein levels were significantly upregulated in HCC cells treated with Pyr (Fig. 3B). This suggests that the mechanism by which Pyr inhibited autophagic flux was not due to a decline in lysosome number. In addition, autophagic flux was assessed in SMMC-7721 cells using red fluorescent protein (RFP)-green fluorescent protein (GFP) tandem fluorescently labeled LC3 after treatment with Pyr or BafA1. As reported previously [39], when autophagosomes fuse with lysosomes, GFP is quenched by the acidic microenvironment (GFP^-). Therefore, a red signal (RFP^+-GFP^-) in the merged images indicates autolysosomes formation, while a yellow signal (RFP^+-GFP^+) in the merged images represents autophagosomes. As shown in Fig. 3C, Pyr or BafA1 treatment markedly induced the colocalization of RFP-GFP, suggesting that Pyr blocked the binding of autophagosomes and lysosomes. As shown in Fig. 3D, P62 showed less mitochondrial

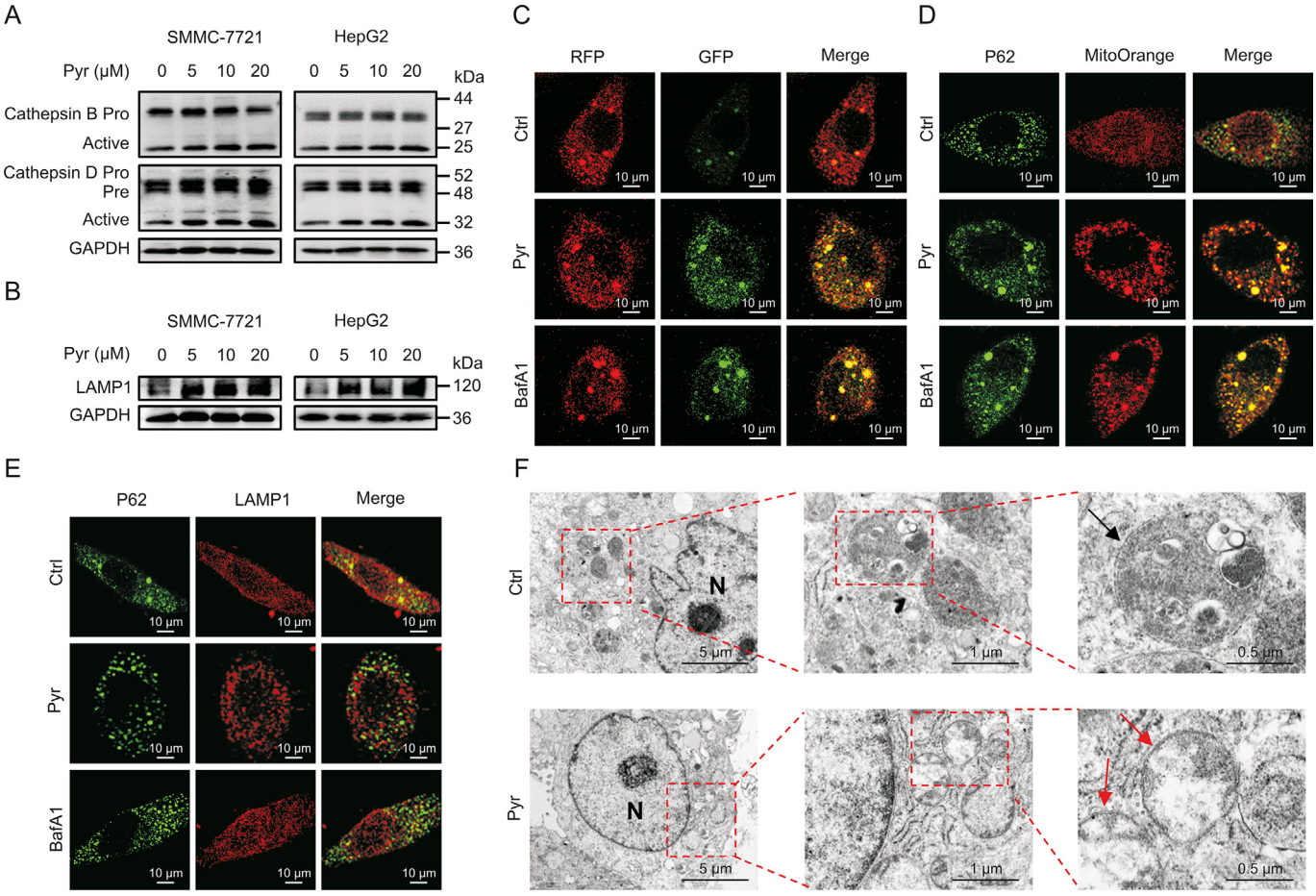

Fig. 3. Pyrimethamine (Pyr) regulates mitophagy by interfering with autophagosome-lysosome formation. (A) Cathepsin B and cathepsin D protein levels in Pyr-treated hepatocellular carcinoma (HCC) cells were assessed by western blotting ($n = 3$). (B) Protein expression of LAMP1 in Pyr-treated HCC cells ($n = 3$). (C) For the evaluation of autophagy flux, red fluorescent protein (RFP)-green fluorescent protein (GFP) tandem fluorescently-tagged light chain 3 (LC3) was stably expressed in SMMC-7721 cells. The cells were treated with 20 μM Pyr or 20 nM bafilomycin (BafA1). RFP, GFP, and 2-channel merged images were evaluated to determine whether autolysosomes were formed. ($n = 3$). (D) SMMC-7721 cells were treated with 20 μM Pyr or 20 nM BafA1. P62 (green), MitoOrange (red), and 2-channel merged images were used to evaluate the colocalization of mitochondria and P62. ($n = 3$). (E) SMMC-7721 cells were treated with 20 μM Pyr or 20 nM BafA1. P62 (green), lysosomal-associated membrane protein 1 (LAMP1) (red), and 2-channel merged images were used to evaluate the colocalization of P62 and LAMP1. ($n = 3$). (F) Representative transmission electron micrographs of HepG2 cells after exposure to 20 μM Pyr for 12 h. The black arrow indicates autolysosomes, and the red arrows indicate autophagosomes. N: nucleus; Mito: mitochondrial fractions; GAPDH: glyceraldehyde 3-phosphate dehydrogenase; Ctrl: control group.

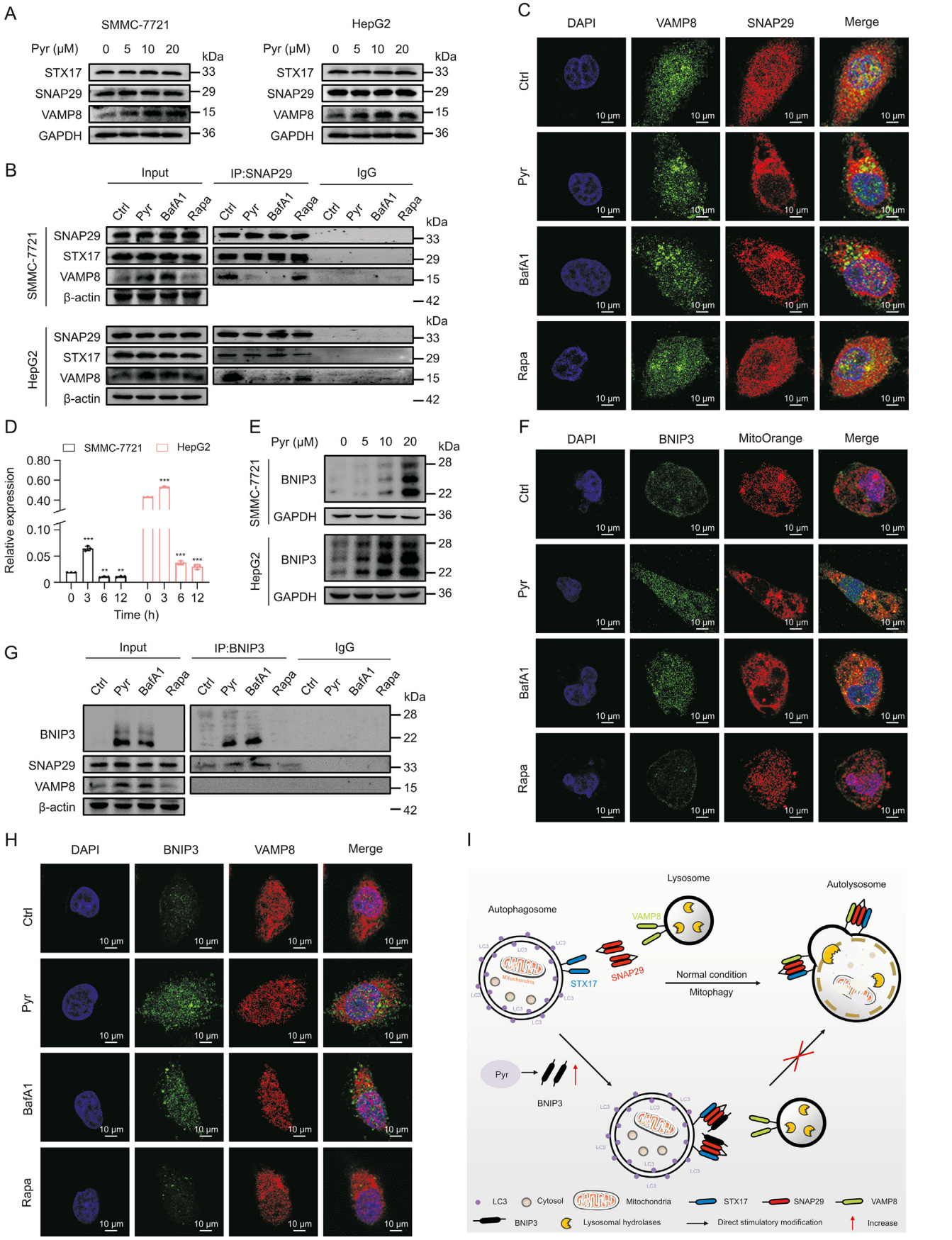

Fig. 4. Pyrimethamine (Pyr) blocks autophagosome-lysosome fusion by inhibiting the interaction of synaptosomal-associated protein 29 (SNAP29) and vesicle-associated membrane protein 8 (VAMP8) by upregulating BNIP3. (A) Hepatocellular carcinoma (HCC) cells were treated with Pyr for 12 h, and the expression levels of syntaxin 17 (STX17), SANP29, and VAMP8 were determined by western blotting ($n = 3$). (B) HCC cells were treated with Pyr (20 μM), bafilomycin (BafA1) (20 nM), or rapamycin (Rapa) (100 nM) for 12 h, and whole-cell lysate was prepared and subjected to immunoprecipitation using anti-SNAP29. The associated SNAP29, STX17, and VAMP8 levels were determined using immunoblotting ($n = 3$). (C) Fluorescence imaging of

colocalization in the control group, while P62 and mitochondrial colocalization considerably increased after Pyr or BafA1 treatment. Fig. 3E showed that P62 strongly colocalized with LAMP1 in the control group, whereas P62 did not colocalize with LAMP1 after Pyr or BafA1 treatment. The above results suggest that Pyr blocked autophagic flux by inhibiting autophagosomes fusion with lysosomes.

In addition, transmission electron microscopy was further used to investigate whether Pyr inhibited autophagosome-lysosome fusion. Consistent with the above results, Pyr-treated HCC cells showed increased autophagosome formation but reduced autolysosome formation in comparison to controls (Figs. 3F and S7). These findings provide definite evidence that Pyr impedes the formation of autolysosome by impairing autophagosome-lysosome fusion rather than affecting lysosome function or reducing lysosome number.

3.5. Pyr blocks autophagosome-lysosome fusion by inhibiting SNAP29-VAMP8 interaction

To further investigate the molecular mechanism of Pyr-inhibited autophagosome-lysosome fusion, the effect of Pyr on the expression of STX17, SNAP29, and VAMP8 was examined, all of which are required for autophagosome-lysosome fusion. As seen in Fig. 4A, VAMP8 levels increased in a concentration-dependent manner after Pyr treatment, whereas Pyr treatment did not influence the levels of SNAP29 or STX17. This phenomenon suggests that Pyr blocked the fusion of autophagosomes and lysosomes not due to a decrease in the expression of these proteins.

Immunoprecipitation assays were performed to further identify whether Pyr influenced the interaction of SNAP29 with VAMP8 or STX17. As shown in Fig. 4B, cell lysates were immunoprecipitated with anti-SNAP29 antibody. Both Pyr and BafA1 treatments reduced the co-precipitation of VAMP8 and SNAP29 compared to the control group. Furthermore, SNAP29-VAMP8 interaction was increased after Rapa treatment. Likewise, immunofluorescence analysis revealed that the colocalization of SNAP29 and VAMP8 decreased upon Pyr or BafA1 treatment, but it increased with Rapa treatment (Fig. 4C). These findings suggest that the Pyr-mediated blockade of autophagosome-lysosome fusion is due to impaired recruitment of SNAP29 to lysosomal VAMP8.

3.6. Pyr upregulates BNIP3 and induces SNAP29-BNIP3 interaction

BNIP3 is a mitophagy receptor that induces cell death and mitophagy [17,40]. Our previous findings indicated that Pyr may influence mitophagy. Thence, the effect of Pyr on the mRNA (Fig. 4D) and protein (Fig. 4E) levels of BNIP3 was investigated. Fig. 4D showed that *BNIP3* mRNA was upregulated at 3 h and downregulated at 12 h post Pyr treatment. However, Pyr treatment of HCC cells for 12 h increased BNIP3 protein levels (Fig. 4E). These results indicate that Pyr may inhibit the protein degradation of BNIP3. Fig. 4F showed that BNIP3 colocalized with mitochondria after Pyr treatment. Expression of BNIP3 has been reported to lead to the accumulation of autophagosomes, but not autolysosomes [19]. In addition, the results of BNIP3 expression were similar to those of Pyr treatment. Therefore, we hypothesized that Pyr-mediated blockade of the fusion of autophagosomes and lysosomes might be associated with BNIP3.

To determine whether BNIP3 is involved in blocking Pyr-mediated autophagosome-lysosome fusion, the interaction of BNIP3 with VAMP8 or SNAP29 in Pyr-treated cells was examined. In cells treated with Pyr or BafA1, BNIP3 co-precipitated with SNAP29 but not with VAMP8. In contrast, BNIP3 did not co-precipitated with SNAP29 or VAMP8 in Rapa-treated cells (Fig. 4G). Further immunofluorescence experiments revealed that cells treated with Pyr, BafA1, or Rapa did not show colocalization between BNIP3 and VAMP8. Notably, BNIP3 fluorescence was stronger in Pyr- and BafA1-treated cells than in untreated cells, which further indicates that Pyr and BafA1 increase BNIP3 expression (Fig. 4H). Additionally, the mechanism by which Pyr blocks autophagosome-lysosome fusion has been identified. (Fig. 4I). Taken together, these results indicate that Pyr may inhibit SNAP29-VAMP8 interaction by upregulating BNIP3 and inducing SNAP29-BNIP3 interaction, thereby blocking the autophagosome-lysosome fusion.

3.7. BNIP3 depletion restores SNAP29-VAMP8 interaction

To examine the role of BNIP3 in Pyr blocking autophagosomes and lysosomes fusion, SMMC-7721 cells were infected with negative control viruses CON077 and LV-BNIP3-RNAi, and then the selected SMMC-7721 cells stably expressing shCon and shBNIP3 using puromycin. Compared to shCon cells, shBNIP3 cells showed reduced Pyr-mediated accumulation of LC3-II (Fig. 5A). Since the inhibition of the interaction between SNAP29 and VAMP8 was involved in the Pyr-mediated blockage of autophagosome-lysosome fusion, the effect of BNIP3 consumption on SNAP29 and VAMP8 co-precipitation was next evaluated by immunoprecipitation experiments. As shown in Fig. 5B, after Pyr treatment, SNAP29 co-precipitation with VAMP8 was not seen in shCon cells, while co-precipitation of SNAP29 and VAMP8 was evident in shBNIP3 cells. To clarify the role of BNIP3 in Pyr-mediated mitophagy, the expression of LC3-II in the mitochondria of shBNIP3 and shCon cells was determined. As shown in Fig. 5C, shBNIP3 cells treated with Pyr showed a reduced accumulation of LC3-II in their mitochondria compared with shCon cells.

Next, SMMC-7721 cells stably expressing shCon or shBNIP3 were inoculated into the underarms of nude mice to construct a nude mouse xenograft tumor model. Figs. 5D–F showed that the growth rate of transplanted tumors in nude mice in the Pyr treatment group was markedly reduced, as was the tumor weight. In addition, the transplanted tumors in the shBNIP3 group were larger than the corresponding shCon group, revealing that *BNIP3* is a tumor suppressor gene. No significant reduction in body weight of experimental animals (Fig. S8), which indicates that Pyr considerably inhibited the growth of HCC cell xenografts with no apparent side effects in this animal study.

To evaluate the effect of BNIP3 depletion on SNAP29 and VAMP8 colocalization *in vivo*, SMMC-7721 xenograft tumor sections were examined by immunofluorescence. Notably, no colocalization of

SMMC-7721 cells immunostained for VAMP8 (green) and SNAP29 (red) and stained with 4'-6-diamidino-2-phenylindole (DAPI) (blue) after treatment with Pyr (20 μM), BafA1 (20 nM), or Rapa (100 nM) for 12 h. $n = 3$. (D) The mRNA levels of *BNIP3* in Pyr-treated HCC cells was determined by reverse-transcription quantitative real-time polymerase chain reaction (RT-qPCR). Data are presented as mean ± standard deviation of the mean (SEM), $n = 3$. $^{**}P < 0.01$, $^{***}P < 0.001$ compared with 0 h. (E) The expression level of BNIP3 in Pyr-treated HCC cells was determined by western blotting ($n = 3$). (F) SMMC-7721 cells were treated with Pyr (20 μM), BafA1 (20 nM), or Rapa (100 nM) for 12 h. The colocalization of MitoOrange (red) and BNIP3 (green) was examined by confocal microscopy. ($n = 3$). (G) SMMC-7721 cells were treated with Pyr (20 μM), BafA1 (20 nM), or Rapa (100 nM) for 12 h, and whole-cell lysate was prepared and subjected to immunoprecipitation using anti-BNIP3 antibody. The associated BNIP3, SNAP29, and VAMP8 levels were determined using immunoblotting ($n = 3$). (H) Confocal microscopy images of SMMC-7721 cells immunostained for BNIP3 (green) and VAMP8 (red) and stained with DAPI (blue) after treatment with Pyr (20 μM), BafA1 (20 nM), or Rapa (100 nM) for 12 h. $n = 3$. (I) The proposed mechanism of the Pyr-mediated blockade of autophagosome-lysosome fusion. Under normal conditions, SNAP29 interacts with STX17 and VAMP8, which drives autophagosome-lysosome fusion. Pyr-mediated upregulation of BNIP3 increases its interaction with SNAP29, which prevents the interaction between SNAP29 and VAMP8, thus blocking autophagosome-lysosome fusion. GAPDH: glyceraldehyde 3-phosphate dehydrogenase; LC3: light chain 3; Ctrl: control group.

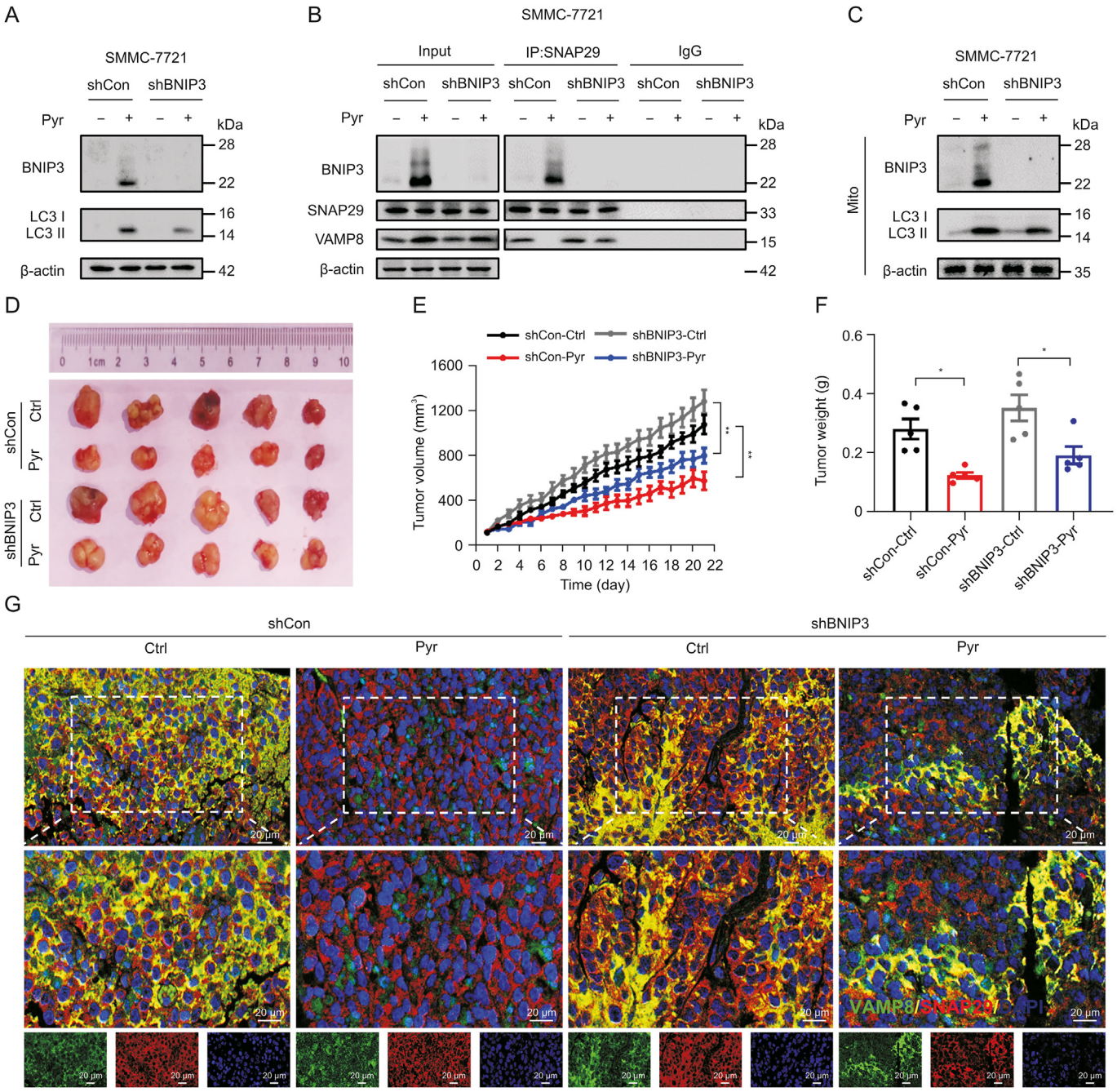

Fig. 5. BNIP3 knockdown attenuates pyrimethamine (Pyr)-mediated blockade of autophagosome-lysosome fusion. (A) SMMC-7721 cells were infected with shCon or shBNIP3 lentivirus. Then the cells were treated with Pyr (20 μM) for 12 h, and the expression of BNIP3, light chain 3 (LC3)-I, and LC3-II were determined by western blotting ($n = 3$). (B) SMMC-7721 cells stably expressing shCon or shBNIP3 were treated with Pyr (20 μM) for 12 h, and whole-cell lysate was prepared and subjected to immunoprecipitation using anti-synaptosomal-associated protein 29 (SNAP29) antibody. Then, the associated BNIP3, SNAP29, and vesicle-associated membrane protein 8 (VAMP8) levels were determined using immunoblotting ($n = 3$). (C) SMMC-7721 cells stably expressing shCon or shBNIP3 were treated with Pyr (20 μM) for 12 h, the mitochondrial fractions (Mito) were prepared, and then BNIP3, LC3-I, and LC3-II in Mito were determined by western blotting. Voltage-dependent anion channel 1 (VDAC1) served as the control ($n = 3$). (D) Images of tumors from the control and Pyr-treated groups in shCon and shBNIP3 xenograft models ($n = 5$). (E) Tumor volume changed throughout the study. Data are represented as mean ± standard deviation of the mean (SEM) ($n = 5$). Compared with the control group (Ctrl), $^{**}P < 0.01$. (F) Tumors were weighed at the end of the experiment. Data are presented as mean ± SEM ($n = 5$). Compared with the ctrl group, $^{*}P < 0.05$. (G) Immunofluorescence staining of shCon and shBNIP3 tumor sections. The three colors of the tumor sections are VAMP8 (pseudo colored; green), SNAP29 (red), and 4'-6-diamidino-2-phenylindole (DAPI)(blue).

SNAP29 and VAMP8 was seen in tumor tissues of the Pyr-treated shCon group, whereas SNAP29-VAMP8 colocalization was markedly increased in tumor tissues of the Pyr-treated shBNIP3 group (Fig. 5G). In summary, these findings demonstrate that BNIP3 depletion rescues SNAP29-VAMP8 interaction and further restores Pyr-mediated autophagosome-lysosome fusion and autophagic flux.

3.8. Synergistic effects of Pyr and Sora combination (PSC) on HCC cell proliferation and apoptosis

It has been reported that blocking mitophagy may restore the sensitivity of HCC cells to Sora [41], and our previous results suggest that Pyr can inhibit mitophagy. Therefore, Pyr and Sora were

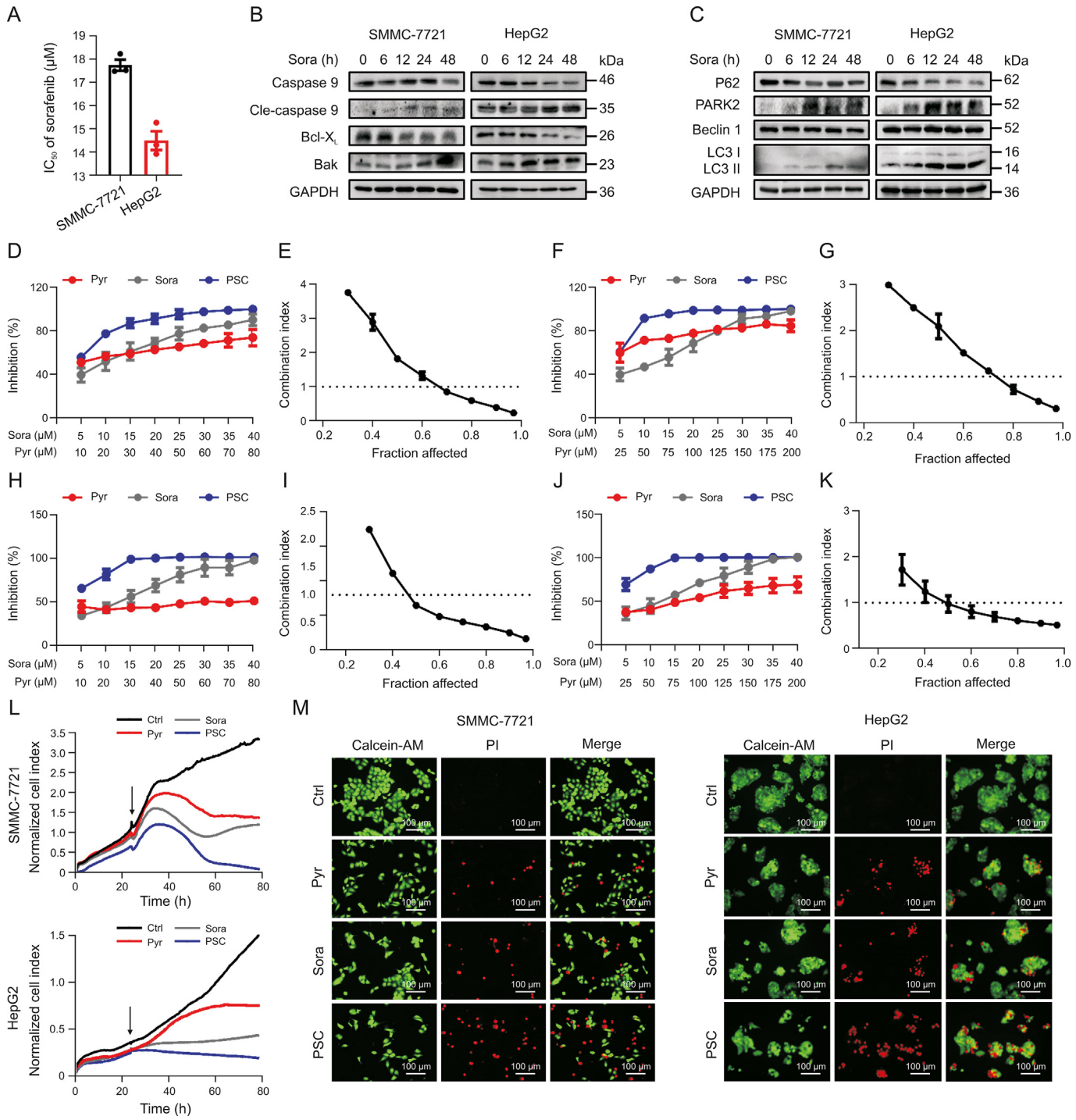

Fig. 6. Synergistic inhibitory effects of pyrimethamine (Pyr) and sorafenib (Sora) combination (PSC) on hepatocellular carcinoma (HCC). (A) HCC cells were treated with Sora, cell viability was determined using the 3-(4,5-dimethylthiazol-2-yl)-2,5-diphenyltetrazolium bromide (MTT) assay, and IC_{50} values were calculated ($n = 3$). (B) The effect of Sora on the expression of apoptosis-related proteins in HCC cells at different time points ($n = 3$). (C) The effect of Sora on the expression of autophagy-related proteins in HCC cells at different time points ($n = 3$). (D) Dose-response study of a 1:2 fixed ratio combination of Sora (5–40 μM) and Pyr (10–80 μM) against SMMC-7721 cells ($n = 3$). (F) Dose-response study of a 1:5 fixed ratio combination of Sora (5–40 μM) and Pyr (25–200 μM) against SMMC-7721 cells ($n = 3$). (H) Dose-response study of a 1:2 fixed ratio combination of Sora (5–40 μM) and Pyr (10–80 μM) against HepG2 cells ($n = 3$). (J) Dose-response study of a 1:5 fixed ratio combination of Sora (5–40 μM) and Pyr (25–200 μM) against HepG2 cells ($n = 3$). (E), (G), (I) and (K) are the ferrous ascorbate (Fa)-carbonyl iron (CI) plots of (D), (F), (H) and (J), respectively, where Fa represents the affected fraction and CI represents the combined index. CI < 1, CI = 1, and CI > 1 denote synergistic, additive, and antagonistic interactions, respectively. Data are represented as mean ± standard deviation of the mean (SEM) ($n = 3$). (L) Real-time cell growth curves of HCC cells treated with Pyr, Sora, and PSC for 78 h ($n = 3$). (M) Representative images of Pyr, Sora, and PSC cytotoxicity against HCC cells, which were assessed by Calcein-AM/propidium iodide (PI) double staining. GAPDH: glyceraldehyde 3-phosphate dehydrogenase; LC3: light chain 3; Ctrl: control group.

combined to investigate their inhibitory effects on HCC cells. Fig. 6A shows the IC_{50} of Sora in the two cell lines. In addition, Annexin V/PI staining (Fig. S9) and immunoblotting experiments (Fig. 6B) revealed that Sora induced apoptosis. Furthermore, cell cycle analysis demonstrated that Sora arrested the cell cycle at G1 phase in HCC cells (Fig. S10).

Consistent with previous reports [42,43], Sora treatment induced autophagy, which may contribute to its decreased clinical efficacy (Fig. 6C). Synergistic effect of Pyr and Sora in SMMC-7721 and HepG2 cells using Chou-Talalay method. According to the Chou-Talalay model [44], the two drugs were combined in the following ratios: Sora:Pyr of 1:2 and 1:5. When the concentration of Sora was 10 μM and the Sora: Pyr ratio was 1:2, the confidence interval (CI) value was less than 1, indicating that Pyr and Sora synergistically inhibited cell growth (Figs. 6D–K). Considering the results of the CI calculation and the inhibition rate of each drug on

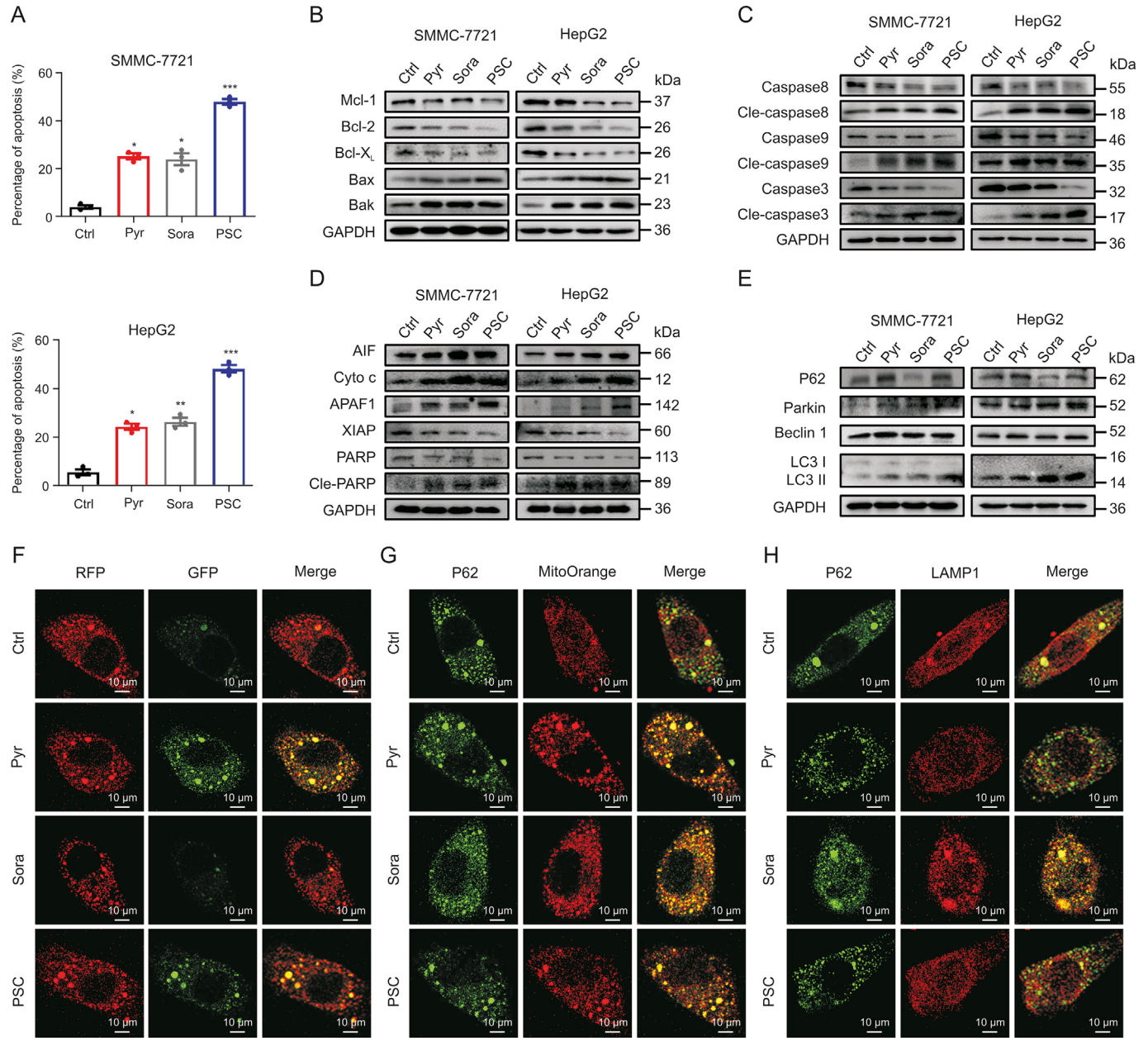

Fig. 7. Pyrimethamine (Pyr) enhances the sensitivity of hepatocellular carcinoma (HCC) cells to sorafenib (Sora) by inhibiting mitophagy. (A) Cell apoptosis was measured by Annexin V/propidium iodide (PI) staining in HCC cells treated with Pyr, Sora, and Pyr and Sora combination (PSC), and the quantitation of apoptotic cells is shown. $^{*}P < 0.05$, $^{**}P < 0.01$, $^{***}P < 0.001$, compared with untreated control cells ($n = 3$). (B–D) HCC cells were treated with Pyr, Sora, and PSC. Apoptosis-related protein expression levels were examined by western blotting ($n = 3$). (E) HCC cells were treated with Pyr, Sora, and PSC. Autophagy-related protein expression levels were examined by western blotting ($n = 3$). (F) For the evaluation of autophagic flux, red fluorescent protein (RFP)-green fluorescent protein (GFP) tandem fluorescent-tagged LC3 was stably expressed in SMMC-7721. The cells were treated with Pyr, Sora, and PSC. RFP (red), GFP (green), and 2-channel merged images were evaluated to determine whether autolysosomes formed. $n = 3$. (G) SMMC-7721 cells were treated with Pyr, Sora, and PSC. MitoOrange (red), P62 (green), and 2-channel merged images were evaluated to determine colocalization of P62 and mitochondria. $n = 3$. (H) SMMC-7721 cells were treated with Pyr, Sora, and PSC. Lysosomal associated membrane protein 1 (LAMP1) (red), P62 (green), and 2-channel merged images were evaluated to determine the colocalization of P62 and LAMP1. $n = 3$. AIF: apoptosis-inducing factor; Cyto c: cytochrome c; APAF1: apoptotic protease-activating factor 1; XIAP: X-linked inhibitor of apoptosis; PARP: poly(ADP-ribose) polymerase; GAPDH: glyceraldehyde 3-phosphate dehydrogenase; LC3: light chain 3; Ctrl: control group.

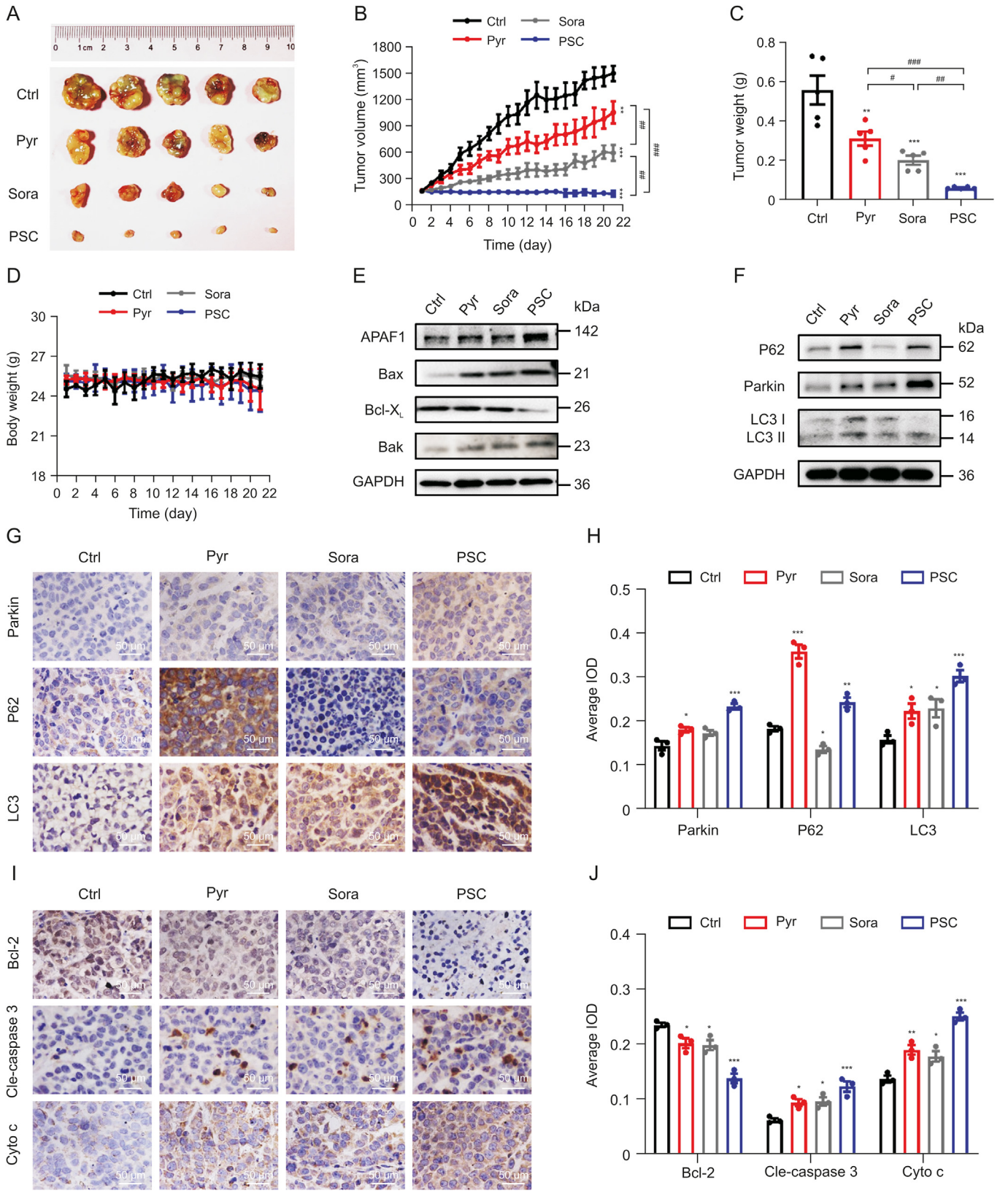

Fig. 8. Pyrimethamine (Pyr) and sorafenib (Sora) combination (PSC) safely inhibits growth of SMMC-7721 cell xenografts in nude mice. (A) Images of the SMMC-7721 cell xenograft model under different treatments ($n = 5$). (B) Tumor volume changes throughout the study. Data are represented as mean ± standard deviation of the mean (SEM) ($n = 5$). Compared with the control group, $^{**}P < 0.01$, $^{***}P < 0.001$; comparison between the corresponding groups, $^{\#\#}P < 0.01$, $^{\#\#\#}P < 0.001$. (C) At the end of the experiment, the tumors were weighed. Data are represented as mean ± SEM ($n = 5$). Compared with the control group, $^{**}P < 0.01$, $^{***}P < 0.001$; comparison between the corresponding groups, $^{\#}P < 0.05$, $^{\#\#}P < 0.01$, $^{\#\#\#}P < 0.001$. (D) Body weight changes throughout the study. Data are represented as mean ± SEM ($n = 5$). (E) Expression levels of apoptosis-associated proteins in SMMC-7721 xenograft tumor samples ($n = 3$). (F) Expression levels of mitophagy-associated proteins in SMMC-7721 xenograft tumor samples ($n = 3$). (G) Immunohistochemical staining of Parkin, P62 and light chain 3 (LC3)

the cells, the selected combined concentrations of Sora and Pyr were 10 μM and 20 μM in HCC cells, respectively. Real-time cell analysis (RTCA) confirmed that PSC markedly inhibited HCC cells growth compared to cells treated with Pyr/Sora alone (Fig. 6L). Calcein-AM/PI double staining experiments also revealed that PSC considerably enhanced the death of HCC cells when compared with the control and standalone Pyr or Sora treatment (Fig. 6M). Next, the effects of PSC on apoptosis (Figs. 7A–D and S11) and the cell cycle (Fig. S12) were examined. Our findings revealed that, compared with a single medication, PSC induced more apoptosis in HCC cells. Furthermore, Sora arrested HCC cells at G1 phase, whereas Pyr arrested HCC cells at S phase. HCC cells were arrested at S phase when Pyr and Sora were combined.

3.9. Pyr enhances the sensitivity of HCC to Sora by inhibiting mitophagy

The expression of P62, Parkin, Beclin 1, and LC3-II/LC3-I was examined in HCC cells treated with Pyr, Sora, and PSC (Fig. 7E). The results indicated that Pyr inhibited autophagy, whereas Sora induced autophagy. Sora-induced autophagy was attenuated after co-treatment with Pyr. Moreover, cells with RFP-GFP tandem fluorescently labeled LC3 were used to further evaluate the above findings. RFP-GFP did not colocalize after Sora treatment, and LC3 showed red puncta (RFP^+-GFP^-). Pyr treatment markedly induced RFP-GFP colocalization, and LC3 is shown as yellow puncta (RFP^+-GFP^+). Similarly, the non-colocalization of RFP-GFP in Sora-treated cells was reversed when Pyr was combined with Sora (Fig. 7F). In addition, after treatment with Pyr, Sora, and PSC, we observed the colocalization of P62 with mitochondria (Fig. 7G) and P62 with LAMP1 (Fig. 7H). The results showed that P62 and mitochondria colocalized after drug treatment, but not in the control group. Furthermore, P62 and LAMP1 colocalized strongly in the Sora treatment group, but not in the Pyr treatment group. The colocalization of P62 and LAMP1 induced by Sora in the PSC group was reversed by Pyr.

A mouse model of SMMC-7721 tumor xenograft was established to evaluate the therapeutic potential of PSC. As shown in Figs. 8A–C, treatment with Pyr or Sora alone showed partial inhibition of tumor growth, but tumor growth was completely inhibited in the PSC group, as evidenced by the reduction in tumor volumes and weights. In addition, body weight did not change significantly after exposure to Pyr, Sora, or PSC (Fig. 8D). The western blotting results confirmed that the PSC group had markedly higher levels of apoptosis in tumor tissues compared with the control and monotherapy groups (Fig. 8E). Additionally, the expression of autophagy-related proteins in the tumor tissues was consistent with the *in vitro* results (Fig. 8F).

Subsequently, immunohistochemical staining of the tumor sections was performed. PSC treatment markedly increased the expression of Parkin and LC3. Pyr treatment increased the expression of P62, whereas Sora treatment inhibited its expression, and Pyr reversed the inhibition of P62 expression by Sora in the PSC group (Figs. 8G and H). Moreover, PSC treatment markedly decreased the expression of Bcl-2, and increased the expression of Cleaved-caspase 3 and Cyto c (Figs. 8I and J). These data suggest that Pyr increased the sensitivity of Sora to HCC by inhibiting mitophagy, thereby synergistically inhibiting the growth of HCC *in vitro* and *in vivo*.

4. Discussion

In the present study, we examined the effect of Pyr on mitophagy in HCC cells and the mechanism of action. We found that the inhibition of mitophagy by Pyr is due to the blockage of autophagosomes and lysosomes fusion. *In vitro* and *in vivo* mechanistic studies demonstrated that Pyr inhibited autophagosomes and lysosomes fusion by upregulating BNIP3 to inhibit SNAP29-VAMP8 interaction. Furthermore, the combination of Pyr and Sora treatment confirmed that Pyr increased the sensitivity of human HCC cells to Sora by inhibiting mitophagy *in vitro* and *in vivo*.

Pyr inhibited HCC cell proliferation and induced apoptosis. Interestingly, cells displayed vacuolization during the treatment of HCC cells with Pyr, a phenomenon associated with autophagy [35]. Therefore, we studied the effect of Pyr on autophagy. The expression of autophagy-related proteins was detected after the combination of Pyr with autophagy inducer or inhibitors, indicating that Pyr was an autophagy activator and could block autophagic flux at the late stage. Additionally, treatment with an autophagy inhibitor increased Pyr-induced cell death and apoptosis, suggesting a protective role for autophagy. In addition, Pyr treatment caused mitochondrial morphological changes and dysfunction. The expression of autophagy-related proteins in mitochondria, and Parkin, a key factor in mitophagy [36], revealed that Pyr both initiated and blocked mitophagy.

Several studies have shown that autophagy can be blocked by targeting different stages of the autophagic process [45]. For example, 3-methyladenine is an early inhibitor of autophagy and is able to block autophagosome formation [46]. At late stage, autophagy can be blocked by impeding autophagosomes and lysosomes fusion or by autolysosome degradation. Different autophagy inhibitors (e.g., BafA1 [47] and CQ [48]) inhibit lysosomal function via a variety of mechanisms, thereby inhibiting late autophagy. By detecting the expression of autophagy-related proteins in HCC after Pyr treatment, we observed that Pyr blocked late autophagy. Next, we examined whether Pyr inhibited autophagy by preventing autophagosome-lysosome fusion or autolysosome degradation. Pyr increased the levels of the mature forms of cathepsin B and D, which suggests that Pyr does not affect autophagy by affecting lysosomal function. The upregulation of LAMP1 expression revealed that Pyr did not inhibit autophagic flux by decreasing the number of lysosomes. The colocalization of RFP-GFP tandem fluorescently-labeled LC3 was markedly induced by Pyr treatment, which suggests that Pyr inhibits autophagosome-lysosome fusion. This finding was also confirmed by the colocalization of P62 with mitochondria, but not LAMP1, which occurred upon Pyr treatment. Notably, increased intracellular autophagosome formation and decreased autolysosome formation were seen in Pyr-treated cells by transmission electron microscopy, which further suggests that Pyr inhibits autophagosomes fusion with lysosomes.

SNARE complexes-mediated fusion is critical for the fusion of autophagosomes and lysosomes [12,13]. Lysosome-localized VAMP8, autophagosome-localized STX17 and SNAP29 are key factors involved in this process [14,49]. Depletion of any of these proteins results in the accumulation of autophagosomes by blocking autophagosome-lysosome fusion [50]. In this study, we found that Pyr treatment upregulated the expression of VAMP8 but did not affect the expression of STX17 and SNAP29. In fact, the blockage of autophagosomes fusion with lysosomes after Pyr treatment was due to the inhibition of SNAP29 and VAMP8 interaction and co-localization by Pyr rather than to the decreased expression of these SNAREs.

Pyr treatment of HCC cells upregulated the expression of BNIP3 but downregulated the mRNA level of *BNIP3* at 12 h. It has been reported that the degradation of BNIP3 is regulated by autophagy [51], and our previous results revealed that Pyr inhibits autophagy.

in SMMC-7721 xenografts. (H) Quantification of Fig. 8G. Data are presented as mean ± SEM, $n = 3$. $^{*}P < 0.05$, $^{**}P < 0.01$, $^{***}P < 0.001$ compared with Ctrl. (I) Immunohistochemical staining of Bcl-2, Cle-caspase 3 and Cyto c in SMMC-7721 xenografts. (J) Quantification of Fig. 8I. Data are presented as mean ± SEM, $n = 3$. $^{*}P < 0.05$, $^{**}P < 0.01$, $^{***}P < 0.001$ compared with Ctrl. GAPDH: glyceraldehyde 3-phosphate dehydrogenase; APAF1: apoptotic protease-activating factor 1; Cyto c: cytochrome c; LC3: light chain 3; Ctrl: control group.

Therefore, the changes in expression of BNIP3 that were observed after Pyr treatment further validate our previous conclusions. It was recently reported that BNIP3 expression induced the accumulation of autophagosomes [19]. In agreement with prior reports, our findings indicate that Pyr-mediated BNIP3 upregulation plays a role in autophagosome accumulation by blocking autophagosome-lysosome fusion. On the one hand, Pyr treatment resulted in increased BNIP3 protein expression and autophagosome accumulation, and impeded autophagosomes fusion with lysosomes by blocking SNAP29-VAMP8 interaction. On the other hand, *in vitro* and *in vivo* studies have revealed that BNIP3 depletion eliminated Pyr-mediated blockade of autophagic flux by restoring SNAP29-VAMP8 interaction. The above results indicate that Pyr inhibits SNAP29-VAMP8 interaction by increasing SNAP29-BNIP3 interaction, leading to blockage of autophagosomes fusion with lysosomes. Furthermore, at the mitochondrial level, we observed that BNIP3 colocalized with mitochondria after Pyr treatment, and that the Pyr-induced accumulation of LC3-II in mitochondria was reduced after BNIP3 depletion. This further confirms that BNIP3 plays an indispensable role in Pyr-mediated mitophagy.

Blockade of mitophagy has been reported to restore HCC cell sensitivity to Sora [41], and our previous results revealed that Pyr is a mitophagy inhibitor. Therefore, we combined Pyr and Sora treatments to evaluate whether the combination increased the sensitivity of HCC cells to Sora by affecting mitophagy. Pyr and Sora synergistically inhibited cell growth. Compared to Pyr or Sora treatment alone, PSC considerably induced apoptosis and inhibited HCC cells growth *in vitro* and *in vivo*. Mechanistically, Pyr enhanced the sensitivity of HCC cells to Sora by inhibiting mitophagy.

5. Conclusion

In summary, this study reveals that Pyr impedes SNAP29-VAMP8 interaction by upregulating BNIP3 in HCC cells, thereby blocking autophagic flux. Both *in vitro* and *in vivo* experiments have revealed that the BNIP3-SNAP29 interaction leads to the blocking of the SNAP29-VAMP8 interaction, which in turn blocks autophagosomes fusion with lysosomes and ultimately leads to autophagosome accumulation. Our findings provide new insights into the mechanism of action of Pyr and imply that Pyr has the potential to be developed as a novel inhibitor of mitophagy. Our findings reveal that PSC displays a synergistic inhibitory effect on HCC *in vitro and in vivo*. Pyr enhances the sensitivity of HCC cells to Sora by inhibiting mitophagy, and these results imply that PSC treatment may be a promising therapeutic option for patients with HCC.

CRediT author statement

Jingjing Wang: Conceptualization, Methodology, Visualization, Formal analysis, Data curation, Writing - Original draft preparation; **Qi Su:** Conceptualization, Supervision, Funding acquisition; **Kun Chen:** Software, Formal analysis, Investigation; **Qing Wu:** Software, Visualization; **Jiayan Ren:** Methodology, Validation; **Wenjuan Tang:** Resources, Visualization; **Yu Hu:** Investigation, Validation; **Zeren Zhu:** Methodology, Validation; **Cheng Cheng**: Methodology, Validation; **Kaihui Tu:** Methodology, Validation; **Huaizhen He:** Investigation, Validation; **Yanmin Zhang:** Supervision, Project administration, Funding acquisition.

Declaration of competing interest

The authors declare that there are no conflicts of interest.

Acknowledgments

This work was supported by the National Natural Science Foundation of China (Grant No: 81903643), the “Young Talent Support Plan” of Xi'an Jiaotong University, the Shaanxi Province Science and Technology Development Plan Project (Grant No.: 2022ZDLSF05-05), the Project of Shaanxi Provincial Administration of Traditional Chinese Medicine (Project No.: 2021-03-ZZ-002), and the Shaanxi Province Science Fund for Distinguished Young Scholars (Grant No: 2023-JC-JQ-59). We also thank Miss Ying Hao of the Instrument Analysis Center of Xi'an Jiaotong University for her assistance with super-resolution confocal microscopy.

Appendix A. Supplementary data

Supplementary data to this article can be found online at https://doi.org/10.1016/j.jpha.2023.05.014.

References

[1] H. Sung, J. Ferlay, R.L. Siegel, et al., Global cancer statistics 2020: GLOBOCAN estimates of incidence and mortality worldwide for 36 cancers in 185 countries, CA. Cancer J. Clin. 71 (2021) 209–249.
[2] Z. Liu, Y. Lin, J. Zhang, et al., Molecular targeted and immune checkpoint therapy for advanced hepatocellular carcinoma, J. Exp. Clin. Cancer Res. 38 (2019), 447.
[3] A. Jindal, A. Thadi, K. Shailubhai, Hepatocellular carcinoma: Etiology and current and future drugs, J. Clin. Exp. Hepatol. 9 (2019) 221–232.
[4] B. Allard, S. Aspeslagh, S. Garaud, et al., Immuno-oncology-101: Overview of major concepts and translational perspectives, Semin. Cancer Biol. 52 (2018) 1–11.
[5] R. Amaravadi, A.C. Kimmelman, E. White, Recent insights into the function of autophagy in cancer, Genes Dev. 30 (2016) 1913–1930.
[6] J.M.M. Levy, C.G. Towers, A. Thorburn, Targeting autophagy in cancer, Nat. Rev. Cancer 17 (2017) 528–542.
[7] F. Janku, D.J. McConkey, D.S. Hong, et al., Autophagy as a target for anticancer therapy, Nat. Rev. Clin. Oncol. 8 (2011) 528–539.
[8] D.J. Klionsky, F.C. Abdalla, H. Abeliovich, et al., Guidelines for the use and interpretation of assays for monitoring autophagy, Autophagy 8 (2012) 445–544.
[9] J. Wang, J. Zhang, Y.M. Lee, et al., Quantitative chemical proteomics profiling of *de novo* protein synthesis during starvation-mediated autophagy, Autophagy 12 (2016) 1931–1944.
[10] J. Zhang, J. Wang, S. Ng, et al., Development of a novel method for quantification of autophagic protein degradation by AHA labeling, Autophagy 10 (2014) 901–912.
[11] N. Mizushima, Autophagy: Process and function, Genes Dev 21 (2007) 2861–2873.
[12] Y. Wang, L. Li, C. Hou, et al., SNARE-mediated membrane fusion in autophagy, Semin. Cell Dev. Biol. 60 (2016) 97–104.
[13] X. Tian, J. Teng, J. Chen, New insights regarding SNARE proteins in autophagosome-lysosome fusion, Autophagy 17 (2021) 2680–2688.
[14] E. Itakura, C. Kishi-Itakura, N. Mizushima, The hairpin-type tail-anchored SNARE syntaxin 17 targets to autophagosomes for fusion with endosomes/lysosomes, Cell 151 (2012) 1256–1269.
[15] M. Onishi, K. Yamano, M. Sato, et al., Molecular mechanisms and physiological functions of mitophagy, EMBO J 40 (2021), e104705.
[16] L. Gu, J. Zhang, D. Liu, et al., Development of artesunate intelligent prodrug liposomes based on mitochondrial targeting strategy, J. Nanobiotechnology 20 (2022), 376.
[17] J. Zhang, P.A. Ney, Role of BNIP3 and NIX in cell death, autophagy, and mitophagy, Cell Death Differ 16 (2009) 939–946.
[18] N. Vasagiri, V.K. Kutala, Structure, function, and epigenetic regulation of BNIP3: A pathophysiological relevance, Mol. Biol. Rep. 41 (2014) 7705–7714.
[19] X. Ma, R.J. Godar, H. Liu, et al., Enhancing lysosome biogenesis attenuates BNIP3-induced cardiomyocyte death, Autophagy 8 (2012) 297–309.
[20] R. Fu, Q. Deng, H. Zhang, et al., A novel autophagy inhibitor berbamine blocks SNARE-mediated autophagosome-lysosome fusion through upregulation of BNIP3, Cell Death Dis. 9 (2018), 243.
[21] K. Liu, J. Lee, J.J. Ou, Autophagy and mitophagy in hepatocarcinogenesis, Mol. Cell. Oncol. 5 (2018), e1405142.
[22] X.H. Lin, B.Q. Qiu, M. Ma, et al., Suppressing DRP1-mediated mitochondrial fission and mitophagy increases mitochondrial apoptosis of hepatocellular carcinoma cells in the setting of hypoxia, Oncogenesis 9 (2020), 67.
[23] Y. Zheng, C. Huang, L. Lu, et al., STOML2 potentiates metastasis of hepatocellular carcinoma by promoting PINK1-mediated mitophagy and regulates sensitivity to lenvatinib, J. Hematol. Oncol. 14 (2021), 16.
[24] 1999 USPHS/IDSA guidelines for the prevention of opportunistic infections in persons infected with human immunodeficiency virus. U.S. Public Health

Service (USPHS) and Infectious Diseases Society of America (IDSA), Infect. Dis. Obstet. Gynecol. 8 (2000) 5–74.
[25] F.P. Mockenhaupt, T.A. Eggelte, T. Böhme, et al., *Plasmodium falciparum* dihydrofolate reductase alleles and pyrimethamine use in pregnant Ghanaian women, Am. J. Trop. Med. Hyg. 65 (2001) 21–26.
[26] M.X. Lin, S.H. Lin, C.C. Lin, et al., *In vitro* and *in vivo* antitumor effects of pyrimethamine on non-small cell lung cancers, Anticancer Res. 38 (2018) 3435–3445.
[27] A.M. Giammarioli, A. Maselli, A. Casagrande, et al., Pyrimethamine induces apoptosis of melanoma cells via a caspase and cathepsin double-edged mechanism, Cancer Res. 68 (2008) 5291–5300.
[28] C. Tommasino, L. Gambardella, M. Buoncervello, et al., New derivatives of the antimalarial drug Pyrimethamine in the control of melanoma tumor growth: An *in vitro* and *in vivo* study, J. Exp. Clin. Cancer Res. 35 (2016), 137.
[29] M.W. Khan, A. Saadalla, A.H. Ewida, et al., The STAT3 inhibitor pyrimethamine displays anti-cancer and immune stimulatory effects in murine models of breast cancer, Cancer Immunol. Immunother. 67 (2018) 13–23.
[30] A. Sharma, N. Jyotsana, C.K. Lai, et al., Pyrimethamine as a potent and selective inhibitor of acute myeloid leukemia identified by high-throughput drug screening, Curr. Cancer Drug Targets 16 (2016) 818–828.
[31] X. Zhou, J. Zhang, X. Hu, et al., Pyrimethamine elicits antitumor effects on prostate cancer by inhibiting the p38-NF-κB pathway, Front. Pharmacol. 11 (2020), 758.
[32] Y. Shi, Mechanisms of caspase activation and inhibition during apoptosis, Mol. Cell 9 (2002) 459–470.
[33] Z. Li, L. Mao, B. Yu, et al., GB7 acetate, a *galbulimima* alkaloid from *Galbulimima belgraveana*, possesses anticancer effects in colorectal cancer cells, J. Pharm. Anal. 12 (2022) 339–349.
[34] Q. Zhang, P. Luo, L. Zheng, et al., 18beta-glycyrrhetinic acid induces ROS-mediated apoptosis to ameliorate hepatic fibrosis by targeting PRDX1/2 in activated HSCs, J. Pharm. Anal. 12 (2022) 570–582.
[35] Y. Qiao, J.E. Choi, J.C. Tien, et al., Autophagy inhibition by targeting PIKfyve potentiates response to immune checkpoint blockade in prostate cancer, Nat. Cancer 2 (2021) 978–993.
[36] D. Narendra, A. Tanaka, D.F. Suen, et al., Parkin is recruited selectively to impaired mitochondria and promotes their autophagy, J. Cell Biol. 183 (2008) 795–803.
[37] L. Guntuku, J.K. Gangasani, D. Thummuri, et al., IITZ-01, a novel potent lysosomotropic autophagy inhibitor, has single-agent antitumor efficacy in triple-negative breast cancer *in vitro* and *in vivo*, Oncogene 38 (2019) 581–595.
[38] H. Iwama, S. Mehanna, M. Imasaka, et al., Cathepsin B and D deficiency in the mouse pancreas induces impaired autophagy and chronic pancreatitis, Sci. Rep. 11 (2021), 6596.
[39] S. Kimura, T. Noda, T. Yoshimori, Dissection of the autophagosome maturation process by a novel reporter protein, tandem fluorescent-tagged LC3, Autophagy 3 (2007) 452–460.
[40] A.H. Chourasia, K.F. MacLeod, Tumor suppressor functions of BNIP3 and mitophagy, Autophagy 11 (2015) 1937–1938.
[41] H. Wu, T. Wang, Y. Liu, et al., Mitophagy promotes sorafenib resistance through hypoxia-inducible ATAD3A dependent Axis, J. Exp. Clin. Cancer Res. 39 (2020), 274.
[42] S. Shimizu, T. Takehara, H. Hikita, et al., Inhibition of autophagy potentiates the antitumor effect of the multikinase inhibitor sorafenib in hepatocellular carcinoma, Int. J. Cancer 131 (2012) 548–557.
[43] B. Zhou, Q. Lu, J. Liu, et al., Melatonin increases the sensitivity of hepatocellular carcinoma to sorafenib through the PERK-ATF4-Beclin1 pathway, Int. J. Biol. Sci. 15 (2019) 1905–1920.
[44] T.C. Chou, Theoretical basis, experimental design, and computerized simulation of synergism and antagonism in drug combination studies, Pharmacol. Rev. 58 (2006) 621–681.
[45] B. Pasquier, Autophagy inhibitors, Cell. Mol. Life Sci. 73 (2016) 985–1001.
[46] Y. Wu, X. Wang, H. Guo, et al., Synthesis and screening of 3-MA derivatives for autophagy inhibitors, Autophagy 9 (2013) 595–603.
[47] A. Yamamoto, Y. Tagawa, T. Yoshimori, et al., Bafilomycin A1 prevents maturation of autophagic vacuoles by inhibiting fusion between autophagosomes and lysosomes in rat hepatoma cell line, H-4-II-E cells, Cell Struct. Funct. 23 (1998) 33–42.
[48] C.A. Homewood, D.C. Warhurst, W. Peters, et al., Lysosomes, pH and the antimalarial action of chloroquine, Nature 235 (1972) 50–52.
[49] K. Hegedűs, S. Takáts, A.L. Kovács, et al., Evolutionarily conserved role and physiological relevance of a STX17/Syx17 (syntaxin 17)-containing SNARE complex in autophagosome fusion with endosomes and lysosomes, Autophagy 9 (2013) 1642–1646.
[50] E. Itakura, N. Mizushima, Syntaxin 17: The autophagosomal SNARE, Autophagy 9 (2013) 917–919.
[51] C.W. Park, S.M. Hong, E.S. Kim, et al., BNIP3 is degraded by ULK1-dependent autophagy via MTORC1 and AMPK, Autophagy 9 (2013) 345–360.